

Frascati Physics Series Vol. nnn (2001), pp. 000-000
HEAVY QUARKS AT FIXED TARGET - Rio de Janeiro, Oct. 9-19, 2000

Rare Decay Results from KTeV and (ρ_{CKM}, η_{CKM})

Leo Bellantoni
Fermi National Accelerator Laboratory
for The KTeV Collaboration

ABSTRACT

Rare decay results from KTeV are reviewed, emphasizing modes that in principle provide information about the CKM matrix. Our recent results in lepton flavor violating modes are also presented.

1 The Data Sample

The KTeV results shown here are from the 1997 data sample, which consists of about 2.7×10^{11} K_L^0 decay samples. KTeV also took data in 1999, giving a total data sample about 2.5 times what is presented here for three body decays and about 3.2 times what is presented here for four body decays. A summary of the KTeV detector is in the Appendix.

2 Modes Relevant for ρ_{CKM}

The decay $K_L^0 \rightarrow \mu^+ \mu^-$ contains a short-distance contribution which depend on the ρ parameter of the Wolfenstein formulation of the CKM matrix. The appropriate diagrams, shown in Fig. 1, correspond to a branching ratio contribution of 1)

$$\mathcal{B}r(K_L^0 \rightarrow \mu^+ \mu^-) = \frac{\alpha^2 \mathcal{B}r(K^+ \rightarrow \mu^+ \nu)}{\pi^2 \sin^4 \theta_W} \frac{\tau(K_L^0)}{\tau(K^+)} \left\{ \left(1 - \frac{\lambda^2}{2}\right) Y_{NL} + A^2 \lambda^4 (1 - \rho) Y_t \right\}^2. \quad (1)$$

where Y_{NL} and Y_t incorporate next-to-leading order QCD corrections, and A and λ are from the Wolfenstein parameterization of the CKM matrix. The important thing to notice here is the dependence on ρ_{CKM} . Unfortunately, there are sizeable long-range contributions, as shown in Fig. 2, as well.

The long distance contribution when both photons are real can be determined with a measurement of $K_L^0 \rightarrow \gamma\gamma$ and a pair of QED vertices. 2, 3) The branching ratio for $K_L^0 \rightarrow \gamma\gamma$ is known about 2.5%. To determine the contribution when one or more of the photons is off-shell requires determination of the form factor for the $K_L \gamma^{(*)} \gamma^{(*)}$ vertex. With that and $\mathcal{B}r(K_L^0 \rightarrow \mu^+ \mu^-)$, which is now known to $\pm 2.2\%$, we can determine the short range contribution to $K_L^0 \rightarrow \mu^+ \mu^-$, and thereby determine ρ_{CKM} . **This is the reason for our interest in the form factor.** After discussing experimental information from KTeV about the form factor in four different modes, I will return to a pressing theoretical issue in this scheme for constraining ρ_{CKM} .

2.1 $K_L^0 \rightarrow \mu^+ \mu^- e^+ e^-$

The decay $K_L^0 \rightarrow \mu^+ \mu^- e^+ e^-$ will allow determination of the $K_L \gamma^{(*)} \gamma^{(*)}$ form factor directly from the mass spectrum of the dilepton pairs. The signal appears as a set of four tracks in the magnetic spectrometer, two of which point to clusters in the calorimeter with energy within $\pm 5\%$ of the momentum measured in the spectrometer, and two of which point to clusters of low energy (we required < 3 GeV) and which extrapolate out to the muon counter $\mu 3$. The major backgrounds are

- $K_L^0 \rightarrow \mu^+ \mu^- \gamma$, with $\gamma \rightarrow e^+ e^-$ through detector interaction. This background is reduced by requiring that the tracks of the charged particles

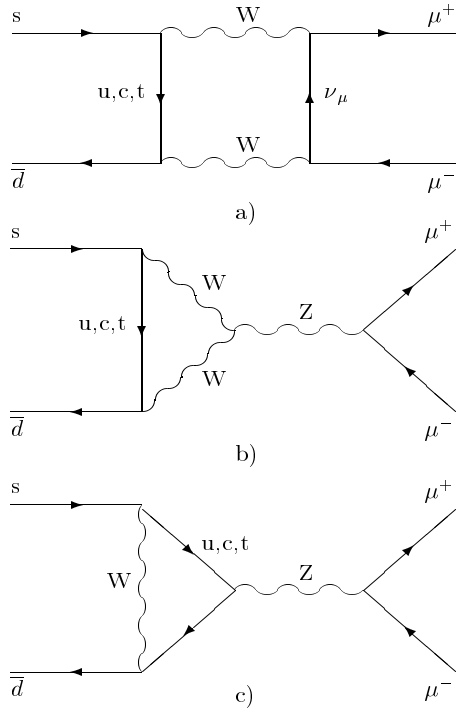


Figure 1: *Interesting short distance contributions to $K_L^0 \rightarrow \mu^+ \mu^-$.*

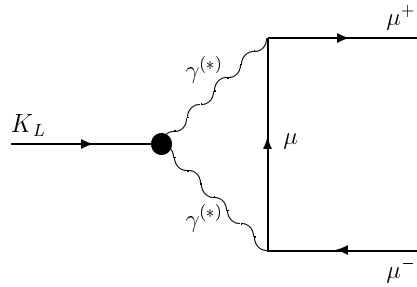


Figure 2: *Boring long distance contributions to $K_L^0 \rightarrow \mu^+ \mu^-$.*

are well separated at the first drift chamber, and that the mass of the e^\pm pair be over 3 MeV. After selection requirements, this background is estimated to be 0.13 events. This estimate uses a Monte Carlo simulation which is well-tuned to the data in regards to electromagnetic interactions in the vacuum window, where nearly all of the important interactions occur.

- $K_L^0 \rightarrow \pi^+\pi^-\pi^0$, with $\pi^0 \rightarrow e^+e^-\gamma$, where both π^\pm fake μ^\pm and the γ goes undetected. As KTeV was designed with minimal detector mass in the tracking system, we have limited ability to detect the kink which should in principle exist for the $\pi^\pm \rightarrow \mu^\pm$ decays which make up the bulk of this misidentification category. However, we can verify that the tracks form a good vertex in the decay region and that the track segments upstream of the magnet are close to the segments downstream of the magnet at the magnet's bend plane. With the simulation, we estimate 0.03 events background from this source. That number includes the contribution from the experimentally similar $K_L^0 \rightarrow \pi^+\pi^-e^+e^-$.
- Events where two simultaneous K_L^0 decays produced four charged particles appearing as an e^+e^- pair and a $\mu^+\mu^-$ pair - for example, two $K_L^0 \rightarrow \pi^\pm e^\mp \nu$ decays with π^\pm that appear as μ^\pm . This background level is estimated at 0.02 events using wrong-sign combinations from the data.

KTeV has made the first observation of $K_L^0 \rightarrow \mu^+\mu^-e^+e^-$, finding 38 events and determining $\mathcal{B}r(K_L^0 \rightarrow \mu^+\mu^-e^+e^-) = (2.50 \pm 0.41 \pm 0.15) \times 10^{-9}$. This preliminary result is in good agreement with the VDM model ²⁾ and differs from both the $\mathcal{O}(p^6)$ χ PT prediction ⁴⁾ and Uy's model. ⁵⁾ With this event sample, although we can make statements about CP violation as in Uy's model, we can not at this time say anything about the form factor. Over a hundred events are expected with the inclusion of the 1999 data.

2.2 $K_L^0 \rightarrow e^+e^-e^+e^-$

The decay $K_L^0 \rightarrow e^+e^-e^+e^-$ provides a much larger sample than $K_L^0 \rightarrow \mu^+\mu^-e^+e^-$ to work with. The signal is similar to the $\mu^+\mu^-e^+e^-$ signal, except of course for the particle identification. The major backgrounds are

- $K_L^0 \rightarrow e^+e^-\gamma$, with $\gamma \rightarrow e^+e^-$ through detector interaction. Similarly, there is the decay $K_L^0 \rightarrow \gamma\gamma$, with two γ conversions. Again, track spac-

ing requirements at the first drift chamber are required. After selection requirements, this background is 3.0 ± 0.3 events.

- $K_L^0 \rightarrow \pi^\pm e^\mp \nu \gamma$, with pair conversion and a π^\pm misidentified as an e^\pm . The primary cause of this misidentification is from π^\pm which go down the beam hole in the calorimeter and have no associated cluster; to keep the signal acceptance high, these events are permitted. Thus, the rate of this background is largely controlled by the geometry of the detector, which is easily modeled in simulation. This background is 0.5 ± 0.5 events.

KTeV's preliminary result is $\mathcal{B}r(K_L^0 \rightarrow e^+ e^- e^+ e^-) = (3.73 \pm 0.18 \pm 0.27) \times 10^{-8}$. This is in good agreement with expectations,⁶⁾ as are certain angular distributions which show indirect CP violation in this mode. With a sample of 436 events (before background subtraction), we can begin to discuss the form factor. However, the radiative corrections for electronic decays need to be handled carefully and our form factor analysis is currently being examined by the collaboration. The branching ratio analysis is limited by systematic uncertainties and is likely to stay that way. The form factor analysis will probably benefit from the improved statistics of the 1999 data.

2.3 $K_L^0 \rightarrow \mu^+ \mu^- \gamma$

The decay $K_L^0 \rightarrow \mu^+ \mu^- \gamma$ provides a still larger sample to work with, albeit with one of the photons on-shell. The signal appears as two vertexable tracks of opposite sign, and a single calorimeter cluster that is unassociated to any track and which combines with the tracks to have a reconstructed mass within 8 MeV of the K_L^0 mass. The background is $K_L^0 \rightarrow \pi^\pm \mu^\mp \nu$, with a π^\pm misidentified as a μ^\pm , and an accidentally coincident calorimeter cluster not associated to any charged particle's track. This cluster is often not a photon; often it is from some other particle, and this background is reduced by requiring that the cluster have a transverse shower profile consistent with that of an electromagnetic shower. These accidental "photons" are typically of low energy, and this background is further reduced by requiring $E_\gamma > 8$ GeV. Interpolating the reconstructed kaon mass distribution from our data using the shape of this distribution from the simulation, we find this background to be 222 ± 15 events. All other backgrounds added together are less than the uncertainty in this estimate.

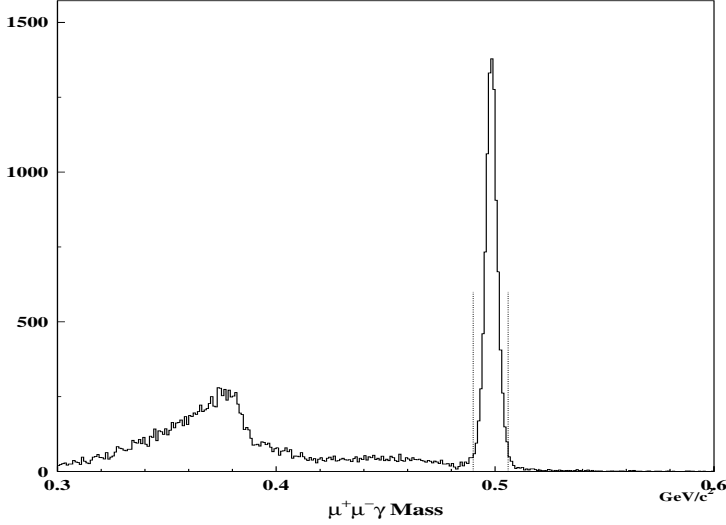


Figure 3: Reconstructed $m_{\mu\mu\gamma}$ distribution after selection criteria. The feature near 380 MeV is from $K_L^0 \rightarrow \pi^+\pi^-\pi^0$; the $K_L^0 \rightarrow \pi^\pm\mu^\mp\nu$ background dominates from ~ 400 – 600 MeV, with a slight enhancement from $K_L^0 \rightarrow \pi^\pm\mu^\mp\nu\gamma$ at 450 MeV.

Figure 3 shows the reconstructed kaon mass distribution. ⁷⁾ There are 9327 events in the mass window $490 < m_{\mu\mu\gamma} < 506$ MeV, and our preliminary result is $\mathcal{B}r(K_L^0 \rightarrow \mu^+\mu^-\gamma) = (3.66 \pm 0.04 \pm 0.07) \times 10^{-7}$. Existing predictions are roughly comparable, but depend greatly on the assumed form factor. The measurement of this decay channel is now limited by systematic uncertainties that will not be reduced by including the 1999 data. With this sample of data in a muonic mode, we can easily make reliable measurements of the form factor.

There are two widely used models of the $K_L\gamma^{(*)}\gamma^{(*)}$ form factor: that of Bergström, Massó and Singer, ⁸⁾ (BMS) and that of D’Ambrosio, Isidori, and Portolés ⁹⁾ (DIP). The first is a vector dominance model with one parameter, α_{K^*} , which quantifies the relative contribution of the vector meson and pseudoscalar diagrams in $K_L \rightarrow \gamma\gamma^{(*)}$ decays. To apply the BMS form to decays with two virtual photons, we use the product of two form factors for single γ^* s. The second model has two parameters, α_{DIP} and β_{DIP} , and has the properties of (a) being consistent with $\mathcal{O}(p^6)$ χ PT, (b) including the poles of vector reso-

nances of arbitrary residues, (c) having parameters that can be experimentally determined in the low- q^2 limit and (d) observing certain constraints from QCD which apply to the high- q^2 limit.

We determine the form factor parameters using the measured branching ratio and the integrated form factors alone. We also measure the form factor parameters by fitting the $m_{\mu\mu}$ distributions; the two methods produce consistent results which we combine, yielding $\alpha_{K^*} = -0.157^{+0.025}_{-0.027}$ and $\alpha_{DIP} = -1.52 \pm 0.09$. Because one of the photons is on-shell, sensitivity to β_{DIP} is identically zero. (In $K_L^0 \rightarrow e^+e^-e^+e^-$, sensitivity to β_{DIP} is practically zero because virtual photons tend to materialize as low mass e^+e^- pairs). With these results in hand, we repeat the analysis of DIP (*op.cit.*), and conclude that $\rho_{CKM} > -1.0$ (BMS form factor) or $\rho_{CKM} > -0.2$ (DIP form factor).

2.4 $K_L^0 \rightarrow e^+e^-\gamma$

This mode provides copious statistics: there will be $\mathcal{O}(10^5)$ events in the 1997 data sample alone. Obviously, systematic uncertainties need to be well understood, and radiative corrections are critical. The analysis of the KTeV data for this mode is underway.

2.5 Discussion of Constraints on ρ_{CKM}

The constraint that we are presently able to set on ρ_{CKM} is not yet as stringent as those that can be set by other means,¹⁰⁾ and it shows strong variation with the model used to extrapolate from $\gamma^*\gamma$ to $\gamma^*\gamma^*$ decays. The resolution of this extrapolation problem should be possible with more data in the $e^+e^-e^+e^-$ and $\mu^+\mu^-e^+e^-$ modes, but another hurdle lies beyond this one.

To fully calculate the contribution from the diagrams in Fig. 2, one needs to understand the form factor in the high- q^2 limit, but from K_L^0 decay data, one can only measure the form factor up to $q^2 \lesssim m_K^2$. There are three important recent papers addressing this issue: that of DIP (*op.cit.*), that of Valencia¹¹⁾ and that of Gómez Dumm and Pich.¹²⁾ It is beyond the scope of this talk to discuss these papers in detail, but it should be noted that (a) Valencia seems to come to a more pessimistic conclusion than the other authors and (b) there does not seem to be a detailed calculation of what form factors permit interesting limits on ρ_{CKM} in the SM scenario or how much theoretical uncertainty will be introduced into a measurement of ρ_{CKM} , should that be possible. In any

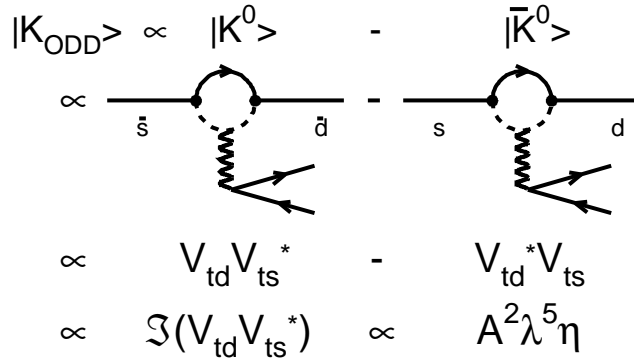


Figure 4: Interesting short distance contributions to $K_L^0 \rightarrow \pi^0 \ell^+ \ell^-$. There are also box diagrams with similar amplitudes.

event, a better understanding of the components of $K_L^0 \rightarrow \mu^+ \mu^-$ may well be of use in setting bounds on possible New Physics scenarios. It is also true that the power of this technology will increase rapidly with better precision on $\mathcal{B}r(K_L^0 \rightarrow \mu^+ \mu^-)$ and $\mathcal{B}r(K_L^0 \rightarrow \gamma \gamma)$; specifically, one wants the most precise value for $\mathcal{B}r(K_L^0 \rightarrow \mu^+ \mu^-) - (11.950 \cdot 10^{-6}) \mathcal{B}r(K_L^0 \rightarrow \gamma \gamma)$. is .

3 Modes Relevant for η_{CKM}

The decays $K_L^0 \rightarrow \pi^0 \ell^+ \ell^-$ have been extensively studied for many years; ¹³⁾ the basic idea becomes evident after drawing the diagrams of Fig. 4. The real parts of the two components of the K_L^0 decay amplitude cancel, leaving an amplitude proportional to η_{CKM} . In the case where the ℓ^\pm is an e^\pm (μ^\pm), there are also amplitudes from indirectly CP violating and CP conserving processes, and backgrounds from radiative (muonic) Dalitz decay of the K_L^0 . The neutrino case is very clean theoretically, and has become the central topic of kaon physics despite formidable experimental obstacles. The KOPIO collaboration at Brookhaven and the KaMI collaboration at Fermilab plan to measure $\mathcal{B}r(K_L^0 \rightarrow \pi^0 \nu \bar{\nu})$. The CKM collaboration at Fermilab plans to measure $\mathcal{B}r(K_L^0 \rightarrow \pi^+ \nu \bar{\nu})$; the charged mode is similar except that the cancellation in Fig. 4 does not occur. Using numbers in reference ¹⁴⁾, one obtains a constraint on $(\eta_{CKM})^2 + [(\rho_{CKM} - 5.40 \pm 0.66)]^2$ rather than upon $|\eta_{CKM}|$ only.

With some oversimplification, we may compare the measurement of CKM elements with semileptonic kaon decay to the measurement of CKM elements with semileptonic b meson decay in the following way. With b mesons, we can extract leptonic coupling constants because we have the HQET symmetry to help us understand the hadronic side; with kaons, we can extract leptonic coupling constants because we have precise experimental data to help us understand the hadronic side. Expressions for $\mathcal{B}r(K_L^0 \rightarrow \pi^0 \nu \bar{\nu})$ and $\mathcal{B}r(K_L^0 \rightarrow \pi^+ \nu \bar{\nu})$ explicitly ¹⁴⁾ contain $\mathcal{B}r(K^+ \rightarrow \pi^0 e^+ \nu)$.

For these channels, the KTeV results presented in this talk have either been published or been accepted for publication ¹⁵⁾ since the conference. All of the searches resulted in limits which are orders of magnitude more stringent than previously available limits, although sensitivities are not yet good enough to see Standard Model physics. For both $\pi^0 e^+ e^-$ and $\pi^0 \mu^+ \mu^-$, backgrounds have begun to limit the experimental reach to $\sqrt{\text{dataset size}}$. The $K_L^0 \rightarrow \pi^0 \nu \bar{\nu}$ triggers were disabled for the 1999 data.

4 Modes relevant for lepton flavor violation

A detector capable of detecting $K_L^0 \rightarrow \mu^+ \mu^- e^+ e^-$, $\pi^0 e^+ e^-$ and $\pi^0 \mu^+ \mu^-$ is also a detector capable of detecting lepton flavor violation.

4.1 $K_L^0 \rightarrow \mu^+ \mu^+ e^- e^-$

There were no wrong sign combination events from the $K_L^0 \rightarrow \mu^+ \mu^- e^+ e^-$ analysis. From this we obtain a preliminary result, $\mathcal{B}r(K_L^0 \rightarrow \mu^+ \mu^+ e^- e^-) < 1.36 \times 10^{-10}$ at the 90% C.L. We simulated signal events with a flat phase-space distribution to calculate the acceptance.

4.2 $K_L^0 \rightarrow \pi^0 \mu^\pm e^\mp$

Searches for this decay complement searches for $K_L^0 \rightarrow \mu^\pm e^\mp$ by being sensitive to new scalar or vector interactions; the two body decay would be the result of a pseudoscalar interaction. The major backgrounds are

- $K_L^0 \rightarrow \pi^\pm e^\mp \nu$, with the π^\pm faking a μ^\pm , and with two accidental "photons". In addition to the types of cuts used in the modes above, this mode may be suppressed by requiring that the momentum transverse to

the K_L^0 line of flight is small. This is the dominant background, contributing 0.61 ± 0.56 events.

- $K_L^0 \rightarrow \pi^\pm e^\mp \nu \gamma$, with the π^\pm faking a μ^\pm , and with only one accidental "photon". The branching ratio is small, and by requiring that the reconstructed neutrino momentum squared in the K_L^0 frame is non-positive, this background can be reduced to less than 0.0054 events.
- $K_L^0 \rightarrow \pi^+ \pi^- \pi^0$, with one π^\pm faking a μ^\pm and the other appearing as an e^\pm . The particle ID power of the calorimeter is augmented with the TRDs for this analysis, and this background is negligible in the signal region. It does however appear at low reconstructed K_L^0 mass.

We found two candidate events, and given the level of uncertainty in our present background estimates, have chosen to not subtract background for our preliminary result. We find $\mathcal{B}r(K_L^0 \rightarrow \pi^0 \mu^\pm e^\mp) < 4.4 \times 10^{-10}$. In terms of a model based on $SU(n)$ family symmetry¹⁶⁾ with couplings equal to g_{EW} , this corresponds to a vector boson of > 44 TeV. In comparing our results to those of Brookhaven E865, one must allow for the ratio of K_L^0 and K^+ lifetimes and for the fact that E865 is far more sensitive to $\pi^+ \mu^+ e^-$ than to $\pi^+ \mu^- e^+$, while KTeV can see both charge combinations well.

5 Appendix: Description of the KTeV Detector

In the 1997 data taking, an 800 GeV proton beam, with typically 3.5×10^{12} protons per ~ 20 second Tevatron spill every minute, was targeted at a vertical angle of 4.8 mrad on a 1.1 interaction length (300 mm) BeO target. Photons were converted by 76 mm of lead immediately downstream of the target. Charged particles were then removed with magnetic sweeping. Collimators defined two $0.25 \mu\text{sr}$ beams that entered the KTeV apparatus 94 meters downstream of the target. About 14×10^7 neutral kaons per second entered the 65 meter vacuum ($\sim 10^{-6}$ Torr) decay region which extended to the first drift chamber. The spectrometer consisted of a dipole magnet and four drift chambers. The drift chambers ranged from $1.28 \times 1.28 m^2$ to $1.77 \times 1.77 m^2$ in size, and had $\sim 100 \mu\text{m}$ position resolution in both horizontal and vertical directions. Helium filled bags occupied the spaces between the drift chambers; the Kevlar reinforced mylar window which sealed off the vacuum region was just upstream of the

first drift chamber, and converted $(2.74 \pm 0.11) \times 10^{-3}$ of the incident photons into e^+e^- pairs. The magnet's field was uniform to $\sim 1\%$ and was mapped to ~ 1 part in 10^4 over the volume of the pole gap; it imparted a 200 MeV horizontal momentum kick. The spectrometer had a momentum resolution of $\sigma(P)/P = 0.38\% \oplus 0.016\%P$, where P is in GeV. The electromagnetic calorimeter consisted of 3100 pure CsI crystals. Each crystal was 500 mm (27 radiation lengths, 1.4 interaction lengths) long. Crystals in the central $1.2 \times 1.2 m^2$ section of the calorimeter had a cross-sectional area of $25 \times 25 mm^2$, and those in the outer region (out to $1.9 \times 1.9 m^2$) had a $50 \times 50 mm^2$ area. The calorimeter's energy resolution for photons was $\sigma(E)/E = 0.45\% \oplus 2\%/\sqrt{E}$, where E is in GeV, and its position resolution was ~ 1 mm. Additional e^\pm/π^\pm separation was provided with eight transition radiation detectors (TRDs) located behind the spectrometer. The TRDs used polypropylene felt for radiators and 80/20% Xenon/CO2 filled MWPC volumes to detect transition radiation. They provided pion rejection factors at 90% electron acceptance which varied between 200::1 and 300::1 through the data taking period. Nine photon veto assemblies (lead scintillator sandwiches of 16 radiation length thickness) detected particles leaving the fiducial volume. Two scintillator hodoscopes in front of the calorimeter were used to trigger on charged particles. The hodoscopes and the calorimeter had two holes (150×150 mm at the calorimeter) to let the neutral beams pass through without interaction. The muon filter, located behind the calorimeter, was constructed of a 100 mm thick lead wall followed by three steel walls of 1.04, 3.04, and 1.03 m thickness. Scintillator planes with 150 mm segmentation in both horizontal and vertical directions ($\mu 3$) were located after the third steel wall. The segmentation was comparable to the multiple scattering angle of 10 GeV muons at $\mu 3$. The pion punch-through probability, including decays downstream of the calorimeter, was determined as a function of momentum from K_{e3} data, and is on the order of a few times 10^{-3} . The data acquisition system reconstructed on the order of 10^5 events of 7 kbyte size per Tevatron spill online, and the results were used to filter the data.

In 1999, the Tevatron spill was extended to ~ 40 seconds and the spectrometer magnet imparted a 150 MeV horizontal momentum kick.

References

1. G.Buchalla and A.J.Buras, Nucl. Phys. **B412**, 106 (1993).

2. C.Quigg and J.D.Jackson, *UCRL Preprint 18487* (unpublished);
3. L.M.Sehgal, Phys. Rev. **183**, 1511 (1969).
4. L.Zhang, J.L.Goity, Phys. Rev. **D57**, 7031 (1998).
5. Z.Uy, Phys. Rev. **D43**, 802 (1991).
6. T.Miyazaki and E.Takasugi, Phys. Rev. **D8**, 2051 (1973).
7. Gene Breese Quinn, A Measurement of the Branching Ratio and Form Factor of $K_L^0 \rightarrow \mu^+ \mu^-$, PhD. Thesis, U. Chicago, June 2000.
8. L.Bergström, E.Massó and P.Singer, Phys. Lett. **B131**, 229 (1983); Phys. Lett. **B249**, 141 (1990).
9. G.D'Ambrosio, G.Isidori, and J.Portolés PL **B423**, 385 (1998).
10. F. Caravaglios, F. Parodi, P. Roudeau, and A. Stocchi, LAL-00-04, hep-ex/0002171; S. Plaszczynski and Marie-Helene Schune, LAL-99-67, hep-ph/9911280.
11. G.Valencia, NP **B517**, 339 (1998).
12. D.Gómez Dumm and A.Pich, PRL **80**, 4633 (1998).
13. *The review* A.R.Barker and S.H.Kettell, BNL-67590, hep-ex/0009024v2 provides an extensive bibliography.
14. G.Buchalla and A.J.Buras Nucl. Phys. **B548**, 309 (1999).
15. A.Alavi-Harati, *et al.*, Phys. Rev. **D61**, 072006 (2000); Phys. Lett. **B447**, 240 (1999); FERMILAB-PUB-00-225-E, hep-ex/0009030; Phys. Rev. Lett. **84**, 5279 (2000).
16. R.Cahn and H.Harari, Nucl. Phys. **B176**, 135 (1980).